Magnetism and spin dynamics of the $S=\frac{3}{2}$ frustrated trillium lattice compound $K_2CrTi(PO_4)_3$

J. Khatua,[1,2] Suheon Lee,[3] Gyungbin Ban [ORCID],[2] Marc Uhlarz,[4] G. Senthil Murugan,[5] R. Sankar,[5] Bassam Hitti,[6] Gerald Morris,[6] Kwang-Yong Choi [ORCID],[2,*] and P. Khuntia [ORCID][1,7,†]

[1]*Department of Physics, Indian Institute of Technology Madras, Chennai 600036, India*

[2]*Department of Physics, Sungkyunkwan University, Suwon 16419, Republic of Korea*

[3]*Center for Artificial Low Dimensional Electronic Systems, Institute for Basic Science, Pohang 37673, Republic of Korea*

[4]*Dresden High Magnetic Field Laboratory (HLD-EMFL), Helmholtz-Zentrum Dresden-Rossendorf, 01328 Dresden, Germany*

[5]*Institute of Physics, Academia Sinica, Taipei 10617, Taiwan*

[6]*Centre for Molecular and Materials Science, TRIUMF, Vancouver, British Columbia V6T 2A3, Canada*

[7]*Quantum Centre of Excellence for Diamond and Emergent Materials, Indian Institute of Technology Madras, Chennai 600036, India*

Competing magnetic interactions, frustration-driven quantum fluctuations, and spin correlations offer an ideal route for the experimental realization of emergent quantum phenomena with exotic quasiparticle excitations in three-dimensional frustrated magnets. In this context, trillium lattice, wherein magnetic ions decorate a three-dimensional chiral network of corner-shared equilateral triangular motifs, provides a viable ground. Herein, we present the crystal structure, dc and ac magnetic susceptibilities, specific heat, electron spin-resonance (ESR), muon spin-relaxation (μSR) results on the polycrystalline samples of $K_2CrTi(PO_4)_3$ wherein the Cr^{3+} ions form a two-coupled trillium lattice. The Curie-Weiss fit of the magnetic susceptibility data above 100 K yields a Curie-Weiss temperature $\theta_{CW} = -23$ K, which indicates the presence of dominant antiferromagnetic interactions between $S = 3/2$ moments of Cr^{3+} ions. For temperatures below 40 K, the Curie-Weiss temperature is reduced to $\theta_{CW} = -3.5$ K, indicative of the appearance of subdominant ferromagnetic interactions. The specific heat measurements reveal the occurrence of two consecutive phase transitions, at temperatures $T_L = 4.3$ K and $T_H = 8$ K, corresponding to two different magnetic phases. Additionally, it unveils the existence of short-range spin correlations above the ordering temperature T_H. The power-law behavior of ESR linewidth suggests the persistence of short-range spin correlations over a relatively wide critical region $(T - T_H)/T_H > 0.25$ in agreement with the specific heat results. The μSR results provide concrete evidence of two different phases corresponding to two transitions, coupled with the critical slowing down of spin fluctuations above T_L and persistent spin dynamics below T_L, consistent with the thermodynamic results. Moreover, the μSR results reveal the coexistence of static and dynamic local magnetic fields below T_L, signifying the presence of complex magnetic phases owing to the entwining of spin correlations and competing magnetic interactions in this three-dimensional frustrated magnet.

I. INTRODUCTION

Frustrated quantum materials, where competing interactions between localized spin moments and frustration-induced strong quantum fluctuations prevent classical Néel order, are highlighted as promising contenders for the discovery of emergent physical phenomena such as quantum spin liquid (QSL), and spin ice with exotic excitations that goes beyond conventional symmetry breaking paradigms in condensed matter [1–4].

A QSL state is a highly entangled state, in which frustration-induced strong quantum fluctuations defy long-range magnetic order even at absolute zero temperatures, despite strong exchange coupling between magnetic moments in the host spin lattice [5–9]. Instead, two spins in the corresponding lattice form resonating spin-singlet pairs

or long-range entangled states with exotic fractionalized excitations such as spinons coupled to emergent gauge fields [10]. Experimental realization of fractional quantum numbers, their identification, and interaction are of profound importance in elucidating the underlying mechanism of some of the groundbreaking phenomena such as high-temperature superconductivity, fractional Hall effect, topological spin textures, and monopoles in quantum condensed matter [11–18] that could have far-reaching ramifications in both fundamental physics and innovative quantum technologies [16]. The realization of QSL state is well established in one-dimensional magnets; however, its identification in higher-dimensional spin systems remains a long-standing challenge in modern condensed matter physics.

In the quest of this long-sought goal, significant effort has been devoted to the exploration of two-dimensional (2D) frustrated lattices [4], which has led to the identification of a few QSL candidates in 2D systems [19,20]. Meanwhile, three-dimensional (3D) frustrated spin lattices such

*choisky99@skku.edu

†pkhuntia@iitm.ac.in

as hyperkagome and pyrochlore lattice are found to host QSL as well. Despite the fact that quantum fluctuations are less pronounced in 3D lattices, certain frustrated 3D lattices, including transition metal-based hyperkagome lattices $PbCuTe_2O_6$ [21,22] and $Na_4Ir_3O_8$ [23,24] along with pyrochlore lattice $NaCaNi_2F_7$ [25–27] as well as rare-earth-based pyrochlore lattice $Ce_2Zr_2O_7$ [28], show signatures of QSL state driven by frustration-induced strong quantum fluctuations [29]. However, the experimental realization of QSL in 3D spin lattices remains scarce, as most of the candidate materials show spin freezing or magnetic ordering owing to perturbing terms in the spin Hamiltonian, lattice imperfections, and exchange anisotropy. In this respect, it is pertinent to investigate promising frustrated magnets on 3D spin lattices wherein competition between emergent degrees of freedom offers an alternate route to stabilize exotic quantum and topological states [4,8,30–32].

To date, hexagonal-based layered frustrated magnets have been studied rigorously for their 2D QSL and certain cubic lattice systems for their 3D counterparts [33]. Recently, there is growing interest in noncentrosymmetric frustrated quantum materials, which crystallize in the cubic space group $P2_13$ [34–36]. The lack of inversion symmetry in such noncentrosymmetric materials gives rise to interesting physical phenomena owing to anisotropic Dzyaloshinskii-Moriya (DM) interactions [34,37–41]. For example, noncentrosymmetric cubic quantum materials are known to host a wide range of quantum phenomena including magnetic skyrmions in insulator $Cu_2OSe_2O_3$ [42], and in itinerant magnets MnSi [43], and FeGe [44], and topological Hall effect in MnGe [45]. Apart from quantum phenomena induced by DM interactions, the spin frustration-induced quantum phenomena in such 3D noncentrosymmetric chiral magnets have garnered significant attention in the quest to achieve distinct quantum phenomena. It is observed that in such quantum materials that crystallizes in the cubic structure ($P2_13$), the magnetic ions form a trillium lattice, i.e., a 3D chiral network of corner-shared equilateral triangular motifs. This lattice provides the origin of spin frustration and may host a myriads of frustration-induced physical phenomena such as QSL. It is a well known that a geometrically frustrated lattice has the potential to harbor frustration-induced new quantum phenomena, as observed in intermetallic compounds. Notable examples include the presence of a dynamic state above the transition temperature in EuPt(Si/Ge) [46], a spin-ice-like state in CeIrSi [47], and the occurrence of pressure-induced quantum phase transitions in MnSi [48].

Nevertheless, oxide-based materials having a single trillium lattice structure are extremely rare. Recently, the trillium lattice, composed of corner-sharing equilateral triangles with six-nearest neighbors, has emerged as an alternative route to further explore the influence of quantum fluctuations in the 3D QSL state and to realize unique quantum phenomena [36,49]. Remarkably, a recent study on the langbeinite family member $K_2Ni_2(SO_4)_3$, which crystallizes in a cubic ($P2_13$) crystal structure, reveals that Ni^{2+} ($S = 1$) ions form a coupled trillium lattice [50]. This material demonstrates several magnetic sublattices with competing magnetic interactions and exhibits a 3D QSL state induced by an applied magnetic field [50]. More recently, continuum spin excitations driven by strong quantum fluctuations are revealed by inelastic neutron

scattering measurement on single crystals of $K_2Ni_2(SO_4)_3$ [51]. Furthermore, despite possessing a high spin moment, the signature of a spin-liquid state has been observed in the trillium compounds $KSrFe_2(PO_4)_3$ (Fe^{3+}; $S = 5/2$) [52] and $Na[Mn(HCOO)_3]$ (Mn^{2+}; $S = 5/2$) [53] that invokes further investigation of the ground state and associated quasiparticle excitations in analogous trillium lattice antiferromagnets. In addition, the spin correlations, interplay between competing interactions and the topology of the electronic band structure in noncentrosymmetric magnets stabilizing in 3D spin lattice, make them an exciting class of materials with potential technological applications [54,55].

Herein, we focus on a phosphate langbeinite $K_2CrTi(PO_4)_3$ (henceforth KCTPO), wherein Cr^{3+} ions with $S = 3/2$ form a two coupled trillium lattice. Magnetization data suggests the presence of dominant antiferromagnetic interactions and subdominant ferromagnetic interactions between $S = 3/2$ moments of Cr^{3+} ions. Specific heat measurements demonstrate two magnetic transitions, namely at $T_L = 4.3$ K and $T_H = 8$ K, as well as the development of short-range spin correlations above T_H, which is supported by critical-like behavior of the ESR linewidth. Furthermore, μSR data uncovers an intriguing evolution of static and dynamic spin correlations, notably below T_L, and a critical slowing down of spin dynamics above T_L. Our experimental findings reveal a complex magnetic landscape with coexisting states, successive phase transitions, and dynamic behavior ($T < T_L$) of Cr^{3+} moments decorating a frustrated 3D trillium spin lattice over a wide temperature regime.

II. EXPERIMENTAL DETAILS

Polycrystalline samples of KCTPO were prepared by a conventional solid-state reaction method. The appropriate stoichiometric amounts of K_2CO_3 (Alfa Aesar, 99.997%), Cr_2O_3 (Alfa Aesar, 99.97%), TiO_2 (Alfa Aesar, 99.995%), and $(NH_4)_2HPO_4$ (Alfa Aesar, 98%) were mixed. Prior to use, the reagent K_2CO_3 was preheated in air at 100 °C to eliminate moisture. The stoichiometric mixture was pelletized, and the pellet was sintered at 300 °C for 4 hrs in an air atmosphere. This sintering procedure was repeated at several intermediate temperatures before annealing the sample at 800 °C for 48 hrs to achieve a single-phase composition. Powder x-ray diffraction (XRD) data were collected using a smartLAB Rigaku x-ray diffractometer with Cu K_α radiation ($\lambda = 1.54$ Å) at room temperature.

Magnetization measurements were performed using the vibrating-sample magnetometer (VSM) option of Physical Properties Measurement System (PPMS, Quantum Design) in the temperature range 2 K $\leqslant T \leqslant$ 300 K and in magnetic fields up to 9 T. To minimize the deleterious effects of magnetic remanence, the sample temperature was set to the paramagnetic temperature region during the intervals between successive isotherm measurements. The ac susceptibility measurements in an oscillating magnetic field with an amplitude of 3 Oe were performed at different frequencies in the temperature range 2 K $\leqslant T \leqslant$ 10 K, using a superconducting quantum interference device VSM (SQUID-VSM, Quantum Design, USA). Specific heat measurements were performed using PPMS by thermal relaxation method in the temperature range 1.9 K $\leqslant T \leqslant$ 250 K and in magnetic fields up to 7 T. High-field magnetization measurement was conducted at Dresden High Magnetic
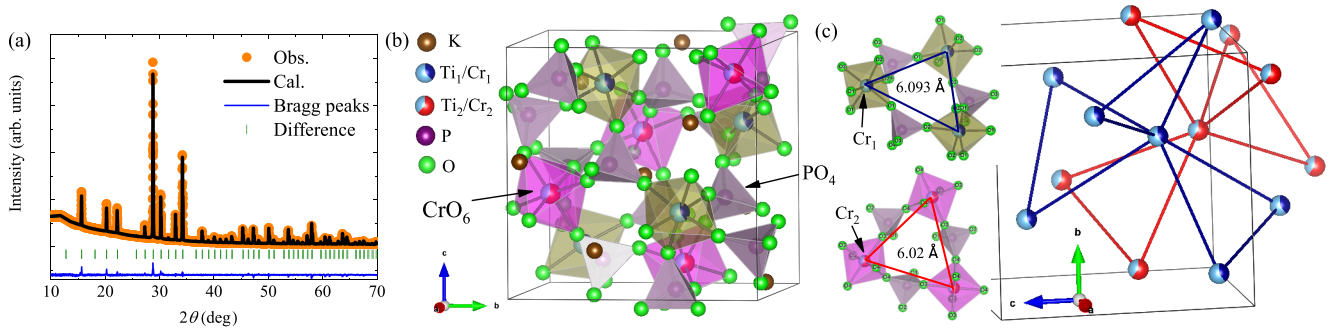
FIG. 1. (a) Rietveld refinement pattern of the room-temperature powder x-ray diffraction data of $K_2CrTi(PO_4)_3$. The orange circle, black line, olive vertical bars, and blue line represent the experimentally observed points, the result of Rietveld fitting, expected Bragg reflection positions, and the difference between observed and calculated intensities, respectively. (b) Schematic depicting the one unit cell of $K_2CrTi(PO_4)_3$. The Cr^{3+} ions form distorted CrO_6 octahedra with dark yellow representing the Cr_1 site and pink for the Cr_2 site, while the P^{5+} ions form PO_4 tetrahedra (light purple). These are connected through a shared oxygen ion, resulting in the formation of a Cr-O-P-O-Cr super-exchange bridge with nearest CrO_6 octahedra. (c) Two coupled trillium lattice of Cr^{3+} ions. Each site of Cr^{3+} ions form a trillium lattice, which is composed of three motifs of equilateral triangle, with bond lengths of 6.093 Å and 6.02 Å corresponding to Cr_1 and Cr_2 sites, respectively. Other atoms are omitted to ensure a clearer view of the trillium lattice and potential nearest-neighbor exchange paths.

Field Laboratory, sweeping a magnetic field up to 30 T at 4 K using a nondestructive pulsed magnet. The obtained data were scaled to the isothermal magnetization taken with PPMS at 4 K.

X-band ($\nu = 9.5$ GHz) electron spin resonance (ESR) measurements were performed using a Bruker EMXplus-9.5/12/P/L spectrometer with a continuous He flow cryostat in the temperature range 4 K $\leqslant T \leqslant$ 300 K. The μ^+SR experiments in zero field and in weak transverse magnetic field (32 G) were performed at the surface muon beamline M20 at TRIUMF in the temperature range 1.93 K $\leqslant T \leqslant$ 80 K. Powder samples (approximately 0.5 g) were placed into a thin envelope composed of Mylar tape coated with aluminum ($\sim$ 50 μm thick), which was mounted on a Cu fork sample stick. A standard ^{4}He flow cryostat was employed to achieve the base temperature of 1.93 K for TRIUMF/M20. The obtained μSR data were analyzed using the musrfit software package [56].

III. RESULTS

A. Rietveld refinement and crystal structure

In order to ensure phase purity and determine atomic parameters of the polycrystalline samples of KCTPO, the Rietveld refinement of powder XRD data was performed using GSAS software [57]. For the Rietveld refinement, the initial atomic parameters were obtained from Refs. [58–60]. The Rietveld refinement reveals that KCTPO crystallizes in a cubic space group ($P2_13$) and the resulting refinement pattern is shown in Fig. 1(a). No secondary phase was found, confirming the successful synthesis of KCTPO in its single phase. The observed sharp and well-defined XRD peaks imply that high-quality polycrystalline samples have been used in this study. The obtained lattice parameters as well as goodness factors from the Rietveld refinement of powder XRD are listed in Table I. Our analysis indicates that among other crystallographic sites in the one unit cell of KCTPO, two crystallographic sites are occupied by magnetic Cr^{3+} ions, which are shared with nonmagnetic Ti^{4+} ions. This could

be attributed to the comparable atomic radii of Cr^{3+} and Ti^{4+}($r_{Cr^{3+}}/r_{Ti^{4+}} = 0.61/0.67$).

Figure 1(b) depicts the one unit cell of KCTPO, where Cr^{3+} ions form distorted CrO_6 octahedra with nearest-neighbor O^{2-} that are separated from adjacent CrO_6 octahedra by PO_4 tetrahedra. The bonding between the CrO_6 octahedra and PO_4 tetrahedra through a common oxygen ion is expected to construct a 3D Cr-O-P-O-Cr superexchange pathway between two nearest-neighbor Cr^{3+} ions (see Table II). Most interestingly, the nearest-neighbor Cr^{3+} ions of each magnetic site form a trillium lattice, i.e., a 3D network of corner-shared equilateral triangular lattice with coordination number six [Fig. 1(c)]. This configuration gives rise to two coupled trillium lattices, potentially serving as a platform for hosting a frustrated spin lattice in 3D.

From a structural point of view, KCTPO belongs to the langbeinite family $K_2M_2(SO_4)_3$ (M = Mg, Co, Ni,..), which crystallizes in the cubic crystal structure (space group

TABLE I. Rietveld refinement of x-ray diffraction data at 300 K yielded structural parameters of $K_2CrTi(PO_4)_3$. (Space group: $P2_13$, $a = b = c = 9.796$ Å, $\alpha = \beta = \gamma = 90°$ and $\chi^2 = 2.228$, $R_{wp} = 4.66\%$, $R_p = 3.24\%$, and $R_{exp} = 3.12\%$.)

Atom	Wyckoff position	x	y	z	Occ.
K_1	$4a$	0.042	0.542	−0.042	1
K_2	$12b$	−0.182	0.317	0.182	1
Cr_1	$12b$	−0.163	0.663	0.336	0.388
Ti_1	$12b$	−0.163	0.663	0.336	0.612
Cr_2	$12b$	0.393	0.606	0.106	0.612
Ti_2	$12b$	0.393	0.606	0.106	0.388
P	$12b$	0.123	0.477	0.292	1
O_1	$12b$	0.100	0.328	0.251	1
O_2	$12b$	−0.010	0.553	0.270	1
O_3	$12b$	0.171	0.486	0.441	1
O_4	$12b$	0.228	0.547	0.202	1

TABLE II. Bond lengths and angles between atoms that result in distinct magnetic interactions between Cr^{3+} spins.

Bond length (Å)	Bond angle (°)
Cr_2-O_3 = 1.961, O_3-P = 1.529	$\angle\ Cr_2$-O_3-P = 131.30
P-O_4 = 1.523, O_4-Cr_2 = 1.952	$\angle\ P$-O_4-Cr_2 = 166.00
Cr_1-O_2 = 1.955, O_2-P = 1.533	$\angle\ Cr_1$-O_2-P = 151.42
P-O_1 = 1.53, O_1-Cr_1 = 1.93	$\angle\ P$-O_1-Cr_1 = 150.41
Cr_1-Cr_1 = 6.093	$\angle\ Cr_1$-Cr_1-Cr_1 = 60
Cr_2-Cr_2 = 6.02	$\angle\ Cr_2$ -Cr_2-Cr_2 = 60

$P2_13$). Two crystallographic $4a$ sites occupy divalent magnetic ions that form a double trillium lattice in the sulfate langbeinites without any antisite disorder [50]. Among various phosphate langbeinites, the recently reported phosphate langbeinite $KSrFe_2(PO_4)_3$ shows a similar configuration, featuring a double trillium lattice with two magnetic sites of Fe^{3+} ions and K/Sr antisite disorder [52]. The aforementioned langbeinite compounds exhibit two interconnected trillium lattices corresponding to two magnetic sites and a complex spin dynamics. To achieve a 3D spin liquid in a simpler system, alternative and more practical approaches can be pursued to explore this phenomenon using a single trillium lattice [35,61]. To accomplish this, substituting nonmagnetic ions for one of the magnetic sites in langbeinite allows for the formation of a single trillium lattice configuration. In this respect, the present family might offer a way to distinguish the magnetic ground state from a double trillium to single trillium lattice similar to that observed in the kagome lattice [62].

B. Magnetic susceptibility

Figure 2(a) depicts the temperature dependence of magnetic susceptibility $\chi(T)$ in several magnetic fields up to 7 T. Upon lowering temperature, a sharp increase of $\chi(T)$ was observed below 10 K, tending to saturate in a magnetic field $\mu_0 H = 1$ T. This behavior indicates the presence of long-range magnetic order in KCTPO consistent with the specific heat result presented in this paper. However, this behavior is suppressed significantly in magnetic fields $\mu_0 H \geqslant 3$ T. A

minor bump around 50 K that appeared in all magnetic fields is attributed to residual oxygen trapped in the polycrystalline sample that was wrapped with teflon during measurement [63]. This signal is not an intrinsic characteristic of the investigated compound in this study.

In order to determine the dominant magnetic interaction between the $S = 3/2$ moments of Cr^{3+} ions, the linear region (100 K $\leqslant T \leqslant$ 300 K) of the $1/\chi(T)$ data in a magnetic field $\mu_0 H = 1$ T was fitted by the Curie-Weiss (CW) law, i.e., $\chi = \chi_0 + C/(T - \theta_{CW})$. Here, χ_0 is the sum of temperature-independent core diamagnetic susceptibility (χ_{core}) and Van Vleck paramagnetic susceptibility (χ_{VV}), C is the Curie constant used to estimate the effective magnetic moment ($\mu_{eff} = \sqrt{8C}\ \mu_B$), and θ_{CW} is the CW temperature associated with the exchange interaction between magnetic moments of Cr^{3+} ions. The corresponding CW fit [red line in the inset of Fig. 2(a)] yields $\chi_0 = -7.42 \times 10^{-4}$ cm^3/mol, C = 1.88 cm^3 K/mol, and $\theta_{CW} = -23 \pm 0.15$ K. The estimated effective magnetic moment $\mu_{eff} = 3.87$ μ_B, is close to the value $g\sqrt{S(S + 1)} = 3.87$ μ_B expected for $S = 3/2$ moments of free Cr^{3+} ions. The negative θ_{CW} indicates the presence of dominant antiferromagnetic interactions between the $S = 3/2$ spin of Cr^{3+} ions. As depicted in the inset of Fig. 2(a), the CW fit begins to diverge below 80 K, signaling the emergence of subdominant ferromagnetic interactions. This is supported by the reduced $\theta_{CW} = -3.5$ K for temperatures below 40 K (not shown here). Interestingly, the material shows anomalies at low temperatures associated with magnetic phase transitions.

To further understand the effect of magnetic fields on the long-range magnetic ordered state in KCTPO, the zero-field-cooled (ZFC) and field-cooled (FC) χ measurements were performed in weak magnetic fields $\mu_0 H \geqslant 0.005$ T. Figure 2(b) reveals the presence of a clear bifurcation between ZFC and FC $\chi(T)$ below the temperature (T_L) = 4.3 K in a magnetic field of $\mu_0 H = 0.005$ T, which implies the presence of a ferromagnetic moment below T_L. Nevertheless, as the magnetic field strength increases, the deviation between ZFC and FC magnetic susceptibility gradually diminishes, almost converging at a magnetic field $\mu_0 H = 0.05$ T.

In order to shed more insights concerning the nature of magnetically ordered phases at different temperature regimes,
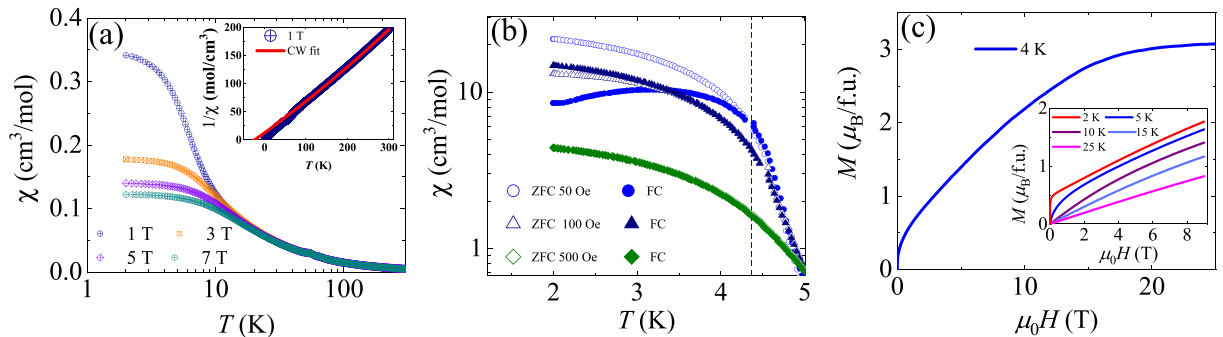

FIG. 2. (a) Temperature dependence of magnetic susceptibility, $\chi(T)$, of $K_2CrTi(PO_4)_3$ in several magnetic fields. The inset depicts the temperature dependence of inverse magnetic susceptibility at $\mu_0 H = 1$ T. The red line represents the Curie-Weiss fits to the high-temperature inverse susceptibility data. (b) Temperature dependence of zero-field cooled (ZFC) and field-cooled (FC) magnetic susceptibility in the temperature range 2 K $\leqslant T \leqslant$ 5 K in magnetic fields 0.005 T $\leqslant \mu_0 H \leqslant$ 0.05 T. The dotted vertical line is at temperature $T_L = 4.3$ K, below which ZFC and FC bifurcation begins in a magnetic field of $\mu_0 H = 0.005$ T. (c) Magnetization as a function of an external magnetic field up to 30 T at 4 K. The inset shows the isotherm magnetization up to 9 T at several temperatures.

isotherm magnetization measurements were performed at several temperatures as shown in the inset of Fig. 2(c). Several features can be observed in the isotherm magnetization curves such as a weak S-shaped curvature in low fields at 2 K, indicating the existence of a ferromagnetic component consistent with the bifurcation between ZFC and FC susceptibility below T_L [64–66]. Notably, the magnetization at 2 K does not reach saturation in a high magnetic field (9 T). The remanent magnetization of $M_r = 0.05$ μ_B/Cr atom and the saturation magnetic moment of about 0.4 μ_B ($\approx 14\%$ of the anticipated full saturation value), deduced from the $M(H, T = 2$ K) curve, negate a simple ferromagnetic ground state. Instead, the linear behavior of the magnetization curves implies the presence of a canted antiferromagnetic state below T_L [67–69]. A similar scenario, attributed to the canted antiferromagnetic phase, has also been observed in several frustrated magnets [70,71]. As the temperature increases, the S-shaped curvature is gradually suppressed due to the quenching of the ferromagnetic component, finally disappearing. The resulting magnetization curve becomes linear at 10 K, indicating the crossover to an additional antiferromagnetic phase. These observations imply that KCTPO exhibits a canted antiferromagnetic state below T_L, above which it hosts an additional antiferromagnetic state corroborated by the specific heat results described below. To find the saturation magnetic moment in high magnetic fields, magnetization measurements were performed at 4 K using a pulsed field magnet up to 30 T.

Figure 2(c) presents the high-field magnetization data at 4 K, calibrated using the VSM-SQUID data at 4 K. It is worth to note that a weak ferromagnetic component persists in low fields $\mu_0 H \leqslant 0.012$ T and beyond this magnetic field, the magnetization continues to increase quasilinearly until $\mu_0 H \leqslant 14$ T and reaches a saturation magnetic moment of 3.04 μ_B in 24 T, which are consistent with dominant antiferromagnetic interactions and subdominant ferromagnetic interactions. We recall that the saturation field is comparable to the CW temperature discussed above. The obtained saturation magnetic moment of 3.04 μ_B is close to the expected theoretical value of 3.0 μ_B per Cr^{3+} ions ($S = 3/2$). The absence of a fractional "1/3" magnetization plateau indicates either the classical behavior of Cr^{3+} spins or the presence of perturbation terms such as magnetic anisotropy and longer-range interactions [72,73].

Before proceeding, we discuss the presence of a ferromagnetic-like saturation plateau instead of a peak in the magnetic susceptibility. Within the canted antiferromagnetic scenario, this feature is explained by a small fraction of ferromagnetic moments arising from canting of the antiferromagnetically ordered moments. As the applied magnetic field increases, these canted moments suppress, leading to a reduction in magnetic susceptibility, similar to the behavior observed in canted antiferromagnets such as La_2ZnIrO_6 [70], $BaFe_2Se_4$ [68], and $Sr_3Ir_2O_7$ [69]. Nonetheless, it is worth to state that a complex magnetic ordering consisting of antiferromagnetic-ferromagnetic mixed structure cannot be totally excluded at the moment. Future neutron diffraction studies are required to resolve this issue.

Figure 3 shows that both the real (χ') and imaginary (χ'') components of ac susceptibility exhibit a well-defined anomaly around 4.4 K, which is consistent with the anomaly
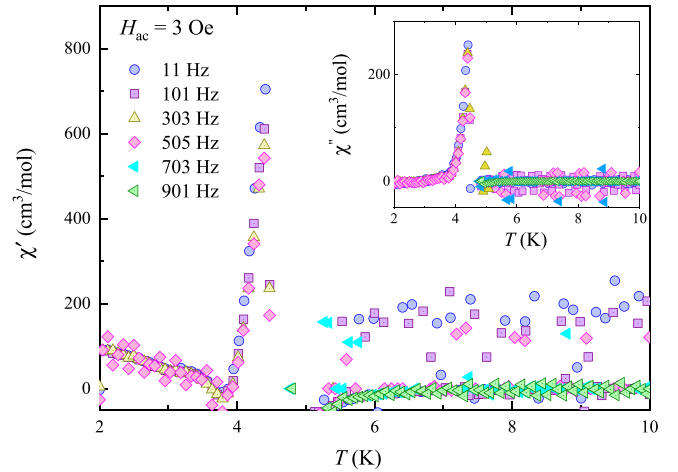

FIG. 3. Temperature dependence of real component (χ') of ac susceptibility at several frequencies where the inset shows the temperature dependence of imaginary component (χ'') of ac susceptibility. An anomaly is observed around 4.4 K.

in specific heat. Moreover, the associated anomaly in ac susceptibility shows no dependence on frequency, providing further evidence that the bifurcation observed in ZFC/FC magnetic susceptibility should not be attributable to spin freezing, but rather to a canted antiferromagnetic state below 4.4 K. All these features suggest the presence of a ferromagnetic-like moment as expected in canted antiferromagnets [74]. On the other hand, the antiferromagnetic phase transition associated with the small entropy release may account for the lack of an identifiable anomaly in the magnetic susceptibility around $T_H = 8$ K, as observed in specific heat [75].

C. Specific heat

Specific heat is an excellent probe to track magnetic order and associated low-lying excitations in frustrated magnets. In order to discern the evidence of magnetic long-range order, temperature-dependent specific heat measurements were performed in several magnetic fields. Figure 4(a) shows the temperature dependence of specific heat in the whole measured temperature range in zero magnetic field. As shown in Fig. 4(b), below $T = 10$ K, the specific heat exhibits two anomalies: one at the temperature $T_L = 4.3$ K and another at the temperature $T_H = 8$ K in zero magnetic field, suggesting the occurrence of successive magnetic phase transitions in KCTPO. It is worth to note that the low-temperature anomaly occurring at T_L in specific heat coincides with the temperature below which the splitting of ZFC and FC χ [Fig. 2(b)], the anomaly in χ' and χ'', as well as the appearance of a ferromagnetic component in magnetization are observed [Fig. 2(c)]. This coincidence suggests that the anomaly at T_L is most likely related to the transition temperature of the canted antiferromagnetic phase in KCTPO. On the other hand, the anomaly at $T_H = 8$ K corresponds to the transition temperature owing to an additional antiferromagnetic phase of KCTPO. We recall that the two successive magnetic phase
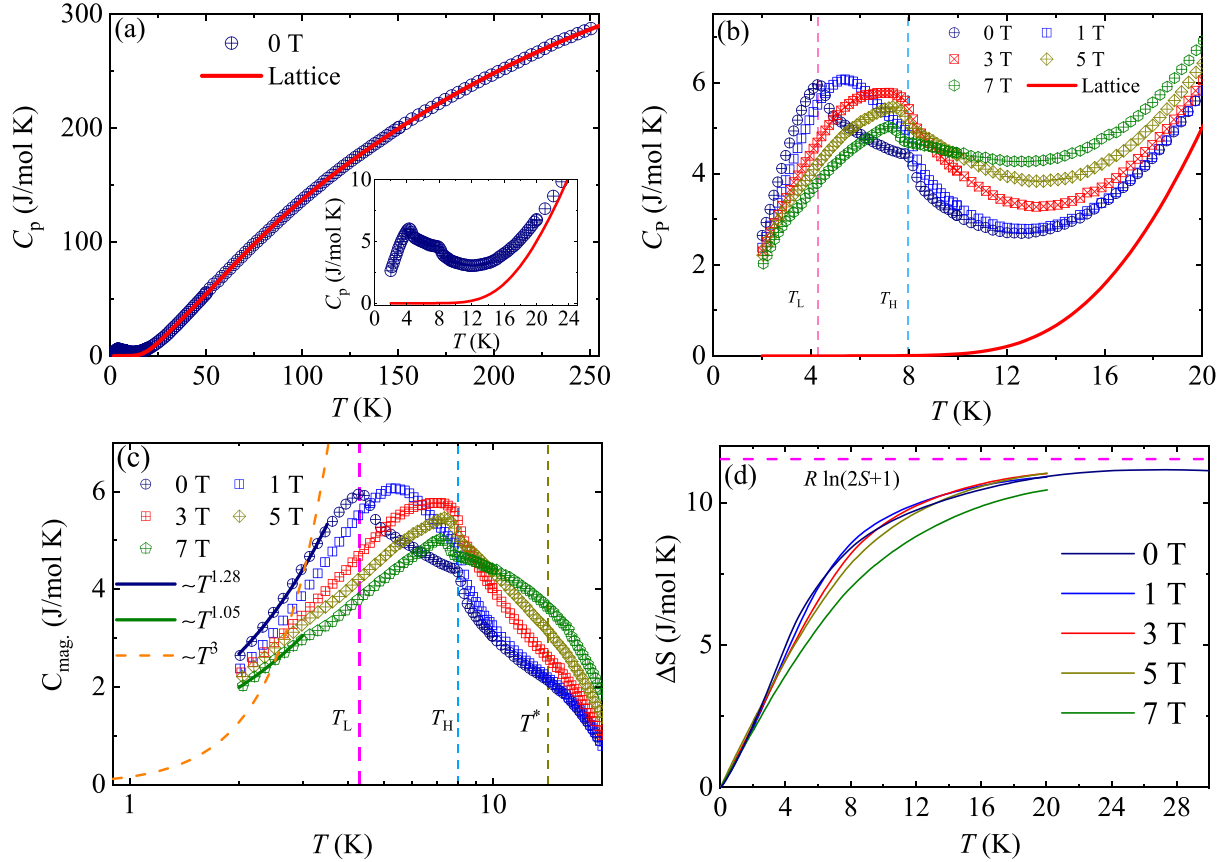
FIG. 4. (a) Temperature dependence of specific heat (C_p) of $K_2CrTi(PO_4)_3$ in zero magnetic field. The solid-red line represents the lattice contributions obtained by combining one Debye and three Einstein functions as described in the text. The inset shows a closer view of the low-temperature specific heat. (b) Temperature dependence of $C_p(T)$ in several magnetic fields in the temperature range 2 K $\leqslant$ T $\leqslant$ 20 K. The dashed-vertical lines indicate two anomalies: one at temperature $T_L = 4.3$ K and another at temperature $T_H = 8$ K in zero field. (c) Temperature dependence of $C_{mag}(T)$ in several magnetic fields in a semi-log scale. Below $T_L = 4.3$ K, the solid lines tentatively represent $\sim T^n$ power-law behavior of the magnetic specific heat, where n varies from 1.3 to 1 in an applied magnetic field of 7 T. The dashed-orange line represents the $C_{mag}(T) \sim T^3$ behavior typical for conventional antiferromagnets. (d) Temperature dependence of entropy change in several magnetic fields with the horizontal pink line indicating the expected entropy of $R\ln(4)$ for $S = 3/2$ spin of Cr^{3+} ions.

transitions are also observed in the two coupled trillium lattice $K_2Ni_2(SO_4)_3$ [50].

Figure 4(b) displays the specific heat in several magnetic fields in the low-temperature regime. The salient observation is that the low-temperature anomaly at T_L shifts towards higher temperatures upon the application of a magnetic field, eventually vanishing at a magnetic field of $\mu_0 H = 3$ T [70]. The increase in T_L with increasing magnetic field can be ascribed to either strong quantum fluctuations or the presence of competing anisotropic interactions [70,76]. While the applied magnetic field increases, the anomaly at T_H widens, shifts to slightly lower temperatures, and a clear λ-like anomaly is observed in $\mu_0 H = 7$ T, suggesting the presence of a typical antiferromagnetic second-order phase transition at T_H in KCTPO. Moreover, in the temperature range 8 K $\leqslant$ T $\leqslant$ 20 K, the specific heat exhibits systematic field dependency, indicating that specific heat is of magnetic origin in this temperature range.

In order to estimate the magnetic entropy and understand the low-temperature magnetic properties relevant to this trillium lattice antiferromagnet, one must subtract the lattice specific heat [$C_{latt}(T)$) from the total specific heat ($C_p(T)$]. To

extract the lattice contributions, we used a combination of one Debye and three Einstein terms, i.e.,

$$C_{latt}(T) = C_D \left[9k_B \left(\frac{T}{\theta_D} \right)^3 \int_0^{\theta_D/T} \frac{x^4 e^x}{(e^x - 1)^2} dx \right]$$
$$+ \sum_{i=1}^3 C_{E_i} \left[3R \left(\frac{\theta_{E_i}}{T} \right)^2 \frac{\exp\left(\frac{\theta_{E_i}}{T}\right)}{\left(\exp\left(\frac{\theta_{E_i}}{T}\right) - 1\right)^2} \right], \quad (1)$$

where θ_D is the Debye temperature, θ_{E_i} represents the Einstein temperatures of the three modes, R and k_B are the molar gas constant and Boltzmann constant, respectively. The corresponding lattice fit, yielding $\theta_D = 223$ K, $\theta_{E_1} = 376$ K, $\theta_{E_2} = 615$ K, and $\theta_{E_3} = 1344$ K, is represented by the solid-red line on top of the experimental data point in Fig. 4(a). In order to minimize the fitting parameters, the coefficients were set at a fixed ratio of $C_D : C_{E_1} : C_{E_2} : C_{E_3} = 1 : 1 : 1.5 : 6$, closely matching with the ratio of the number of heavy atoms (K, Cr, Ti, P) to light atoms (O) in KCTPO.

After subtraction of the lattice contributions, the obtained temperature dependence of magnetic specific heat $C_{mag}(T)$ is shown in Fig. 4(c). As the temperature decreases in a zero

magnetic field, C_{mag} increases and exhibits an inflection point around temperature $T^* = 14$ K, followed by a weak kink at T_H. The broad maximum is attributed to the presence of short-range spin correlations [50]. The presence of a moderate frustration parameter f, roughly estimated through the ratio $f = |\theta_{CW}|/T_H \approx 3$, could account for both the short-range order and the suppression of magnetic order. The anomaly at T_H is relatively weak compared to the anomaly at T_L, similar to the observed anomalies in $K_2Ni_2(SO_4)_3$ [50]. Nevertheless, upon increasing the magnetic field, the canted antiferromagnetic phase diminishes, leading to an increase in the anomaly observed at T_H in $\mu_0H = 7$ T. Most notably, as shown in Fig. 4(c), the magnetic specific heat follows $C_{mag} \sim T^n$ ($n = 1.28$) power law in zero field for temperatures below T_L, which significantly deviates from the $C_{mag}(T) \sim T^3$ behavior typical of conventional antiferromagnets. In the presence of a magnetic field up to 7 T, the average value of n was found to be 1.10. It is worth noting that in future low-temperature specific heat measurements are required to confirm whether the power-law behavior persists even in the sub-Kelvin temperature range. In contrast to KCTPO, the trillium lattice structure with two interpenetrating sublattices of $K_2Ni_2(SO_4)_3$, well below the transition temperature, the magnetic specific heat follows $C_{mag} \sim T^2$ behavior [50].

To quantify the entropy release associated with phase transitions and spin dynamics, it is crucial to account for the magnetic-specific heat below 2 K. In the absence of no more phase transition below 2 K, we extend the corresponding power law to zero temperature. Next, the entropy was obtained by integrating C_{mag}/T with respect to temperature, as shown in Fig. 4(d). The obtained saturation entropy is found to be 11.16 J/mol K at 30 K that is close the theoretically expected value of 11.52 J/mol K for $S = 3/2$ moments. The missing $\sim 3.12\%$ entropy is ascribed to either the existence of short-range magnetic correlations well above the transition temperature or an overestimation of the lattice contribution given the limitations of the model employed here [77,78]. Additionally, around the transition temperature T_H of 8 K, approximately 76% of the saturation entropy is released, suggesting that roughly 20% originates from short-range spin correlations that begin forming as high as at $\sim 3T_H$. However, the lack of a few percentage of entropy because of short-range order persisting above the transition temperature is typical for frustrated magnets [77,79]. This observation is corroborated by the ESR results presented in the following subsection.

D. Electron spin resonance

To provide microscopic insights into the temperature evolution of spin correlations, we conducted X-band ESR measurements down to 4 K [80]. The obtained ESR spectra at several temperatures are shown in Fig. 5(a), which fits well with a derivative of a Lorentzian curve above 8 K. This indicates that the ESR signal is exchange narrowed. At temperatures below $T = 10$ K, the spectra cannot be fitted by a single Lorentzian curve, indicating the development of antiferromagnetic resonance mode and supporting the conclusions drawn from our thermodynamic results. The temperature dependence of estimated g factors from the fit

is shown in Fig. 5(b). Above $T = 100$ K, the obtained g value remains relatively constant at approximately $g = 1.972$, slightly lower than the standard $g = 2$ for a free Cr^{3+} ion. This value is typical for a less-than-half-filled Cr^{3+} ion with a negligible spin-orbit interaction in an octahedral ligand coordination, as observed in similar compounds [78]. The g factor starts to decrease with temperature below 100 K, which corresponds to the deviation from the CW fit [see the inset of Fig. 2(a)]. This is attributed to the persistent magnetic correlations up to several $|\theta_{CW}|$, often observed in frustrated magnets [79].

The ESR linewidth is directly proportional to the spin correlations in transition metal-based systems with minimum spin-orbit coupling. Figure 5(c) shows the estimated ESR linewidth (ΔH_w) of KCTPO as a function of reduced temperatures $T_{rl} = (T - T_L)/T_L$ in the bottom x axis and $T_{rh} = (T - T_H)/T_H$ in the upper x axis. Above the transition temperature T_H, the observed linewidth exhibits a power-law behavior of $T_{rl}/T_{rh} \sim T^{-p}$ in two distinct temperature ranges. For temperatures spanning from 10 K to 24 K, the power exponent p takes values of 0.097 and 0.072, while in the range 30–100 K, the values of p are 0.035 and 0.032 for T_{rl} and T_{rh}, respectively [78,79,81,82]. The critical-like broadening in the temperature range $10 \text{ K} \leqslant T \leqslant 24$ K, alongside the weak hump at T^* in C_{mag} and the small percentage of entropy released above 8 K, supports the notion of the critical-like spin fluctuations. Conversely, the broadening observed in the temperature range $30 \text{ K} \leqslant T \leqslant 100$ K is ascribed to cooperative paramagnetic behavior between the $S = 3/2$ spin of Cr^{3+} ions. Additionally, a deviation from the Curie-Weiss fit has also been noted below 100 K [refer to Fig. 2(a)]. The presence of two-stage broadening is also observed in other high-spin-based frustrated magnets, alluding to the two-step thermal evolution of magnetic correlations [79,81,82].

E. Muon spin relaxation

To capture the microscopic details of spin dynamics and the internal magnetic field distribution, μSR measurements were performed on polycrystalline samples of KCTPO in zero field (ZF) and weak transverse field (wTF). When a weak transverse field (here $B_{TF} = 32$ G) is applied perpendicular to the initial direction of the muon spin polarization, the implanted muon spin precesses around the applied transverse field in the paramagnetic state of the sample, leading to an oscillatory signal with a frequency of $\gamma_\mu B_{TF}/2\pi$, where $\gamma_\mu = 2\pi \times 135.5$ MHz/T represents the muon gyromagnetic ratio [83]. In addition, when a static magnetic field is present in the sample, the muon spin polarization exhibits a nonoscillatory signal, as observed in the material under investigation [77,84,85]. Figure 6(a) shows the evolution of the TF spectra at selected temperatures that were fitted according to

$$A_{wTF}(t) = A_0 f \cos(\gamma_\mu B_{TF} t + \phi) e^{-\lambda_{TF} t} + (1 - f) A_0 e^{-\lambda_L t},$$

(2)

which combines an exponentially decaying oscillatory component, corresponding to muon spins experiencing zero static field, and an exponentially decaying nonoscillatory component that accounts for the component of the static local
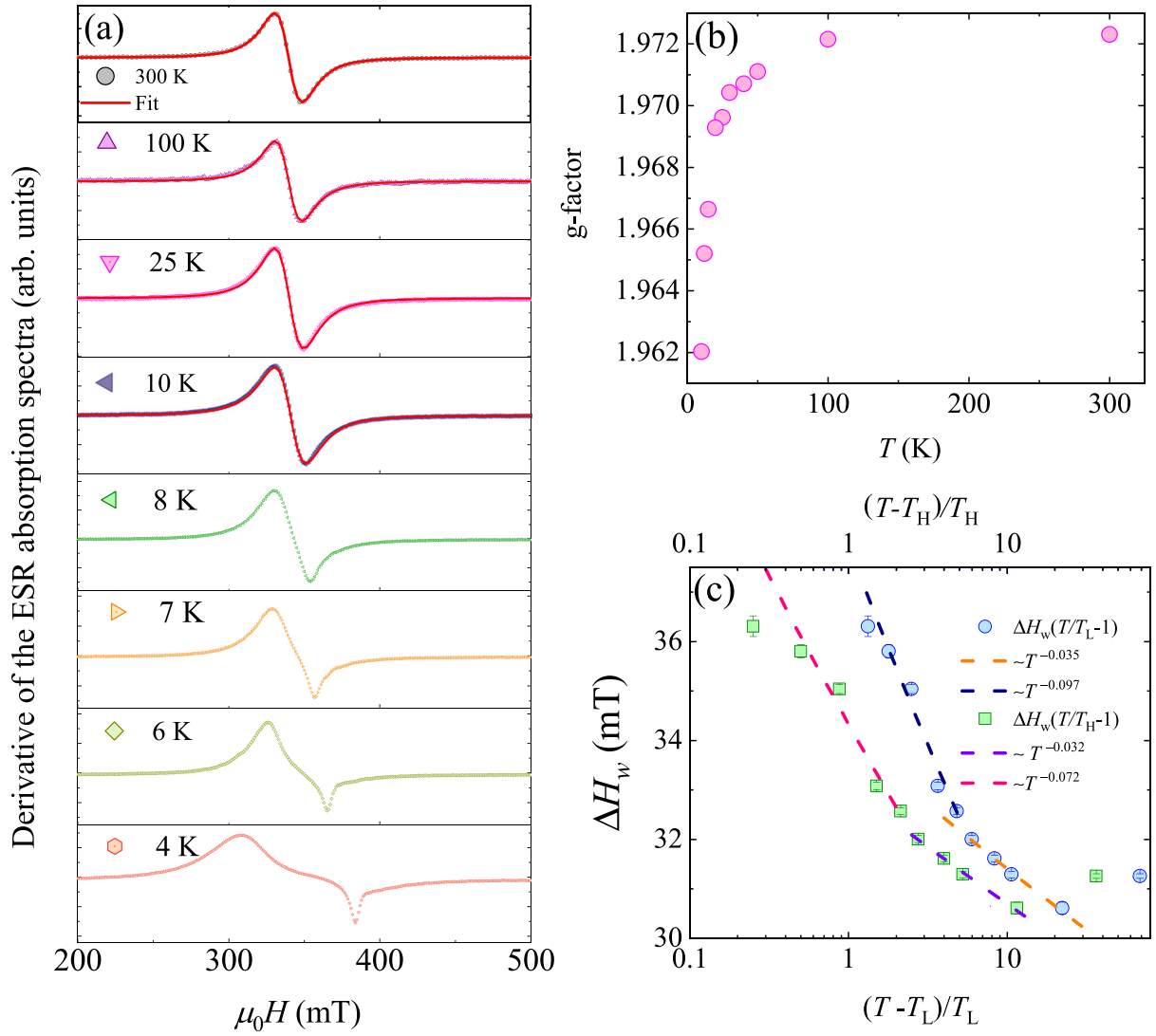
FIG. 5. (a) Derivative of the ESR absorption spectra of $K_2CrTi(PO_4)_3$ at selected temperatures. The solid-red lines indicate the fitting to the Lorentzian line shape above 8 K. (b) Temperature dependence of g factor in a semi-log scale. (c) Semi-log plot of the ESR linewidth ΔH_w as a function of the reduced temperature expressed as $T_{rl} = (T - T_L)/T_L$ on the bottom x axis and $T_{rh} = (T - T_H)/T_H$ on the upper x axis. The dashed lines are power-law fits.
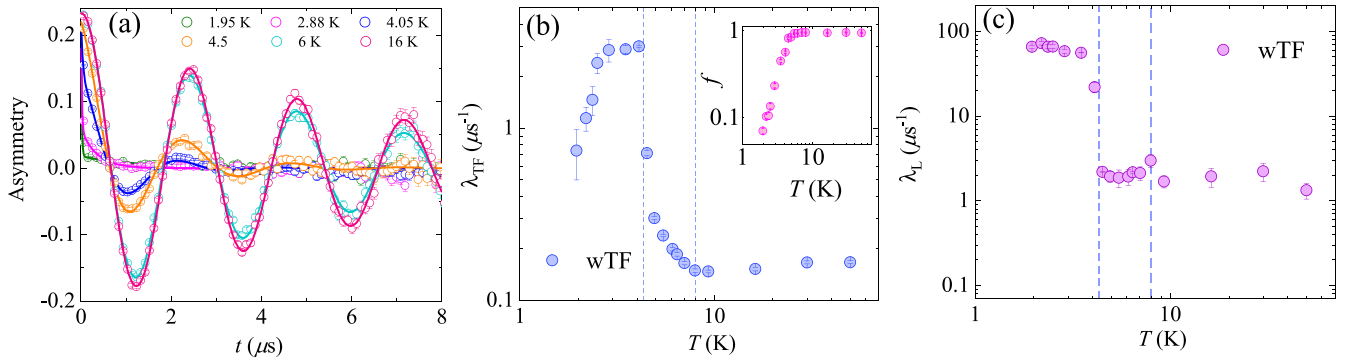
FIG. 6. (a) Time dependence of the muon asymmetry in $K_2CrTi(PO_4)_3$ in a weak transverse field ($B_{TF} = 32$ G) at several temperatures. The solid lines are fits obtained using Eq. (2). (b) Temperature dependence of the muon spin relaxation rate in transverse applied field on a double logarithmic scale. The inset shows the fraction of the oscillating component as a function of temperature. (c) Temperature dependence of the muon spin relation rate due to internal magnetic field in the investigated sample. The dashed-vertical lines indicate the position of characteristic transition temperatures at $T_L = 4.3$ K and $T_H = 8$ K.
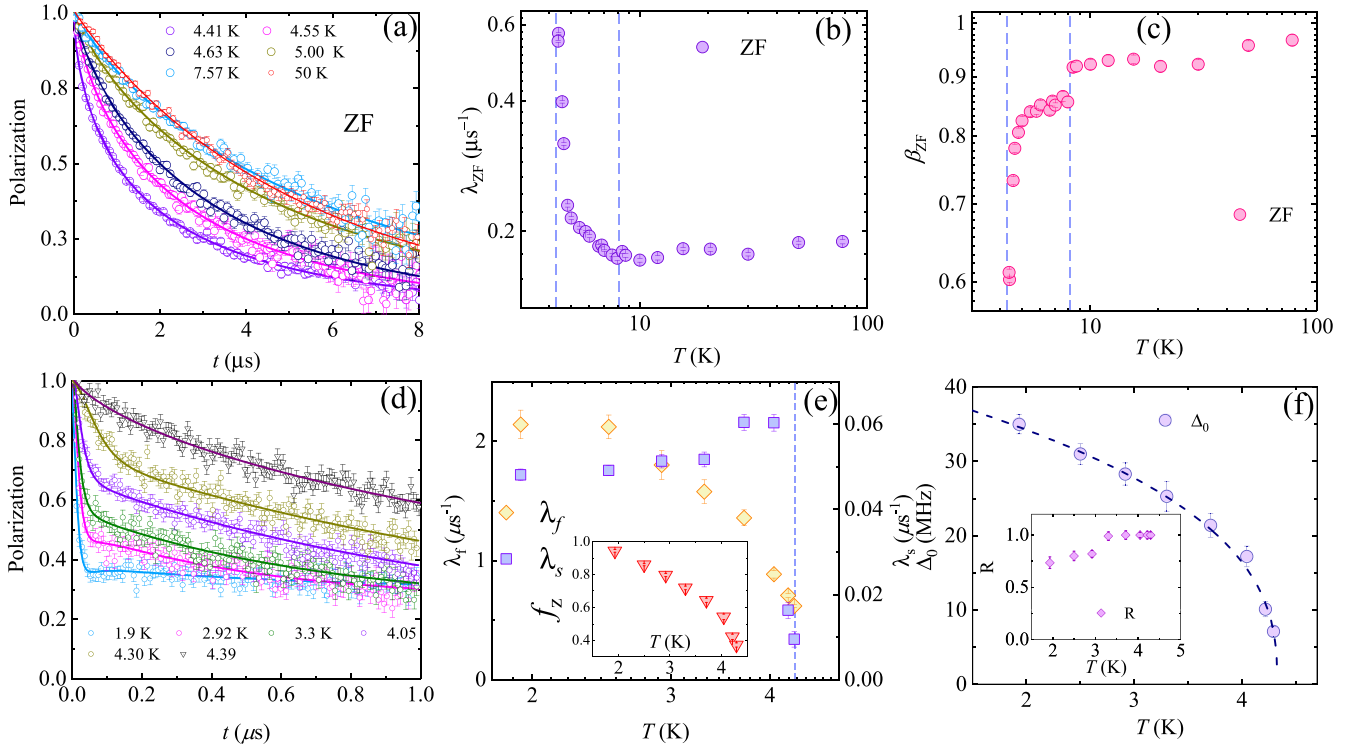
FIG. 7. (a) Time dependence of zero-field μSR spectra of K$_2$CrTi(PO$_4$)$_3$ at temperatures higher than the temperature of canted antiferromagnetic phase transition. The solid lines represent the fitted curve by a stretched exponential function. [(b), (c)] Temperature dependence of the muon spin relaxation rate and stretched exponent as a function of temperature in zero magnetic field on a double logarithmic scale. The dashed-vertical bars indicate the position of characteristic transition temperatures at $T_L = 4.30$ K and $T_H = 8$ K. (d) Time evolution of zero-field spectra at temperatures below the canted antiferromagnet state. The solid lines are the fits of Eq. (3) to the data. (e) Temperature dependence of the fast (left y axis) and slow (right y axis) muon spin relaxation rates on a double logarithmic scale. Inset depicts the temperature dependence of the fraction of quasistatic order with the slow relaxation rate. (f) Mean value of the Gaussian-broadened Gaussian distribution as a function of temperature where the solid lines are the fitted curves with critical scaling behavior of internal field distribution with critical exponent $\beta = 0.37$. Inset shows the temperature dependence of R, i.e., the ratio of the width of distributions (W) to the distribution mean(Δ_0).

field parallel to the initial muon polarization. In Eq. (2), A_0 represents the initial asymmetry at time zero, ϕ denotes the relative phase, λ_{TF} stands for the muon spin relaxation rate in the applied transverse field, and f quantifies the fraction of the oscillatory component while λ_L refers to the muon spin relaxation rate caused by the internal magnetic fields. At short timescales, we observe a significantly damped signal with decreasing temperature without any loss of initial asymmetry, which is a characteristic signature of a magnetically ordered state in KCTPO.

The estimated fraction of the oscillatory signal f, associated to the volume fraction experiencing zero static field [inset of Fig. 6(b)], remains constant to a value of 0.93 in the temperature range 4.3 K $\leqslant T \leqslant 78$ K. This temperature independent value of $f < 1$ is attributed to the presence of weak static local fields above 4.3 K, which is also observed in ESR results. However, it gradually decreases below $T_L = 4.3$ K, indicating a crossover to another magnetically ordered state. It is noteworthy that f does not sharply drop to zero below the transition temperature T_L, suggesting the existence of dynamic local fields in the ordered state. Upon lowering the temperature, the transverse field muon spin relaxation rate gradually increases [see Fig. 6(b)], as expected in the extreme motional narrowing limit of fluctuating magnetic moments. A sharp peak in λ_{TF} at T_L indicates the critical slowing down of

spin fluctuations above the transition temperature as evident from unsaturated magnetic entropy. The notable observation is the occurrence of the critical spin relaxation below T_H [46]. Conversely, the muon spin relaxation rate caused by the static local field [Fig. 6(c)] exhibits a weak kink at T_H, attributed to the antiferromagnetic phase transition similar to that observed in specific heat. This is followed by a rapid rise towards T_L, indicating the enhancement of internal field fluctuations through spin reconfiguration to the canted antiferromagnetic state. It is interesting to note that, below T_L, the λ_{TF} remains constant down to 1.93 K without displaying a sharp fall, persistent spin fluctuations even in the magnetically ordered state, similar to that observed in coupled trillium lattice K$_2$Ni$_2$(SO$_4$)$_3$ [50].

To validate the spin dynamics in the ordered states, ZF-μSR measurements were performed in the wide temperature range. Figure 7(d) shows the ZF-μSR spectra at temperatures above T_L without any change of the initial asymmetry. Furthermore, despite an anomaly in specific heat associated to the magnetic phase transition, the absence of any oscillation or a strong damped signal even in short timescale, suggests that a dynamical behavior of electronic spins associated with the magnetic phase similar to that observed in trillium lattice antiferromagnet K$_2$Ni$_2$(SO$_4$)$_3$. The corresponding μSR data (Fig. 7) can be well fitted to the phenomenological model $P(t) = A_0 \, e^{-(\lambda_{ZF}t)^{\beta_{ZF}}}$, where A_0 is the initial asymmetry, λ_{ZF}

is the muon spin relaxation rate in zero field and β_{ZF} is the stretched exponent. The estimated relaxation rate exhibits several features as shown in Fig. 7(b). Upon lowering the temperature from 78 K, the λ_{ZF} remains constant in the temperature range 8 K $\leqslant T \leqslant$ 78 K. The essentially same behavior is observed by λ_{TF} [see Fig. 6(b)]. Below 8 K, the λ_{ZF} shows a rapid increase, ascribed to the presence of the canted antiferromagnetic phase transition accompanied by a critical slowing down of spin fluctuation consistent with our wTF-μSR results. The obtained stretched exponent, measuring the distribution of electronic moment, is shown Fig. 7(c). At high temperatures, β_{ZF} is close to one, corresponding to the fast fluctuation limit. As the temperature decreases, the β_{ZF} value gradually decreases, notably dropping to 0.85 at $T_H \sim$ 8 K. Below 8 K, the β_{ZF} value gradually decreases, but there is a sudden drop at T_L to a value of 0.6. It is observed that the ZF-μSR data (for $T \geqslant 4.41$ K) cannot be accurately fitted using a single exponential function ($\beta_{ZF} = 1$) or models with multi-exponential components [79]. The obtained $\beta_{ZF} < 1$ is associated with the presence of a distribution of relaxation times, as expected when various spins fluctuate in different timescales due to competing magnetic interactions in KCTPO. The observed β_{ZF} of 0.6 ($>1/3$) value, as seen in Fig. 7(c), implies that the splitting in ZFC and FC χ data at 4.3 K is due to canted antiferromagnetic phase rather than spin freezing [86].

Figure 7(d) displays the time evolution of ZF-μSR spectra at several temperatures below 4.5 K in the short timescale. As the temperature decreases below 4.5 K, the polarization initially exhibits a moderate departure from stretched exponential behavior [87]. As it reaches around 1.9 K, it undergoes an abrupt transition into a strongly nonexponential signal. The shorter time domain clearly shows a substantially damped signal, making it challenging to simulate the muon polarization throughout the whole temperature range using a stretched exponential relaxation function. Furthermore, the absence of any peak in the first Fourier transform of the corresponding spectra indicates that the damped signal cannot be attributable to coherent oscillations typically observed in long-range ordered magnets [85,88,89]. Instead, it suggests the existence of disordered static moments of Cr^{3+} ions below 4.3 K. After attempting with several models [90–92], it turns out that the ZF-μSR data can be modeled with the following polarization function

$$P_{ZF} = f_z P_{GDG}(t; \Delta_0, W)e^{-\lambda_s t} + (1 - f_z)e^{-\lambda_f t}, \quad (3)$$

which takes into account a phenomenological Gaussian-broadened Gaussian (GBG) function with a slow exponential decay with relaxation rate λ_s and a fast exponential decay with relaxation rate λ_f [93,94]. The parameter f_z defines the fraction of quasistatic order in the sample, while the remaining part contributes to dynamic fields. The following GBG polarization function

$$P_{GBG}(t) = \frac{1}{3} + \frac{2}{3}\left(\frac{1}{1 + R^2\Delta_0^2 t^2}\right)^{3/2}\left(1 - \frac{\Delta_0^2 t^2}{1 + R^2\Delta_0^2 t^2}\right)$$
$$\times \exp\left[-\frac{\Delta_0^2 t^2}{2(1 + R^2\Delta_0^2 t^2)}\right] \quad (4)$$

is an extension of the Gaussian Kubo-Toyabe function with a Gaussian distribution width W and a mean value Δ_0, where $R = W/\Delta_0$. This function is commonly employed when the internal field distribution exceeds the Gaussian field distribution. It effectively captures the existence of disordered static magnetic moments with short-range correlations as observed in 3D hyperkagome compound such as $Na_4Ir_3O_8$, which exhibits ZFC and FC splitting in dc susceptibility similar to the compound studied here [24]. The extracted temperature dependence of the fast relaxation rate (λ_f; left y axis), representing a few fraction of Cr^{3+} moments exhibiting dynamic behavior, and the slow relaxation rate (λ_s; right y axis) corresponds to the remaining fraction Cr^{3+} moments displaying static behavior are shown in Fig. 7(e). Both λ_f and λ_s start to increase below T_L and attain a constant value at low temperatures, indicating the coexistence of static and dynamic components of Cr^{3+} moments in KCTPO.

In KCTPO, the origin of static moments can be associated to the canted antiferromagnetic phase involving a small fraction of static Cr^{3+} moments [see the inset of Fig. 7(e)]. Simultaneously, the rest of the Cr^{3+} moments maintain a dynamic state most likely due to the interplay of competing magnetic interactions. In geometrically frustrated magnets, the coexistence of dynamic and static electronic moments is a common scenario, as also observed in two coupled trillium lattice $K_2Ni_2(SO_4)_3$ and pyrochlore lattice $NaCaNi_2F_7$ [27]. It should be mentioned that the GBG polarization function effectively describes the spin dynamics of quantum magnets featuring inhomogeneous static magnetic moments owing to the random distribution of magnetic sites [94,95]. This scenario is applicable to the current compound KCTPO attributed to the presence of Cr/Ti antisite disorder. The mean value of the local field distribution Δ_0 undergoes an order-parameter-like decrease as the temperature increases from 1.9 K towards T_L. It may be noted that the relative distribution width R steadily increases and reaches a value of one at T_L [inset of Fig. 7(f)]. The critical-like behavior of the local field distribution near T_L is described by phenomenological expression [95,96] $\Delta_0(T) = \Delta_0(T = 0 \text{ K})[1 - \frac{T}{T_L}]^\beta$ that yields $\beta = 0.37$ that is typical for 3D Heisenberg magnets [see the dashed line in Fig. 7(f)]. Using $\Delta_0 = 35$ MHz at $T = 1.9$ K, the calculated internal magnetic field is found to be $\langle B_{loc} \rangle \approx 400$ G. In order to confirm such static magnetic field is of electronic origin, we also performed μSR measurements at 3.3 K in longitudinal field (not shown here), which decouples the static field owing to nuclear origin. It is observed that approximately 2 kG $> \langle B_{loc} \rangle$ longitudinal field is required to recover full polarization, confirming the presence of both dynamic and static moments of Cr^{3+} ions in KCTPO. Similar to KCTPO, the observed muon spin asymmetry of triangular lattice antiferromagnet $NiGa_2S_4$ was characterized by a stretched exponential function at high temperatures, associated to multichannel relaxation, while the data at low temperatures were primarily influenced by static local fields [87]. The contrasting time evolution of the muon spin polarization function, observed both above and below the characteristic temperature of T_L, may be associated with distinct magnetic phases in KCTPO, similar to those found in other 3D frustrated magnets [97–100].

IV. CONCLUSIONS

In summary, we have thoroughly investigated the structural and magnetic properties of nearly perfect $S = 3/2$ trillium lattice $K_2CrTi(PO_4)_3$ through magnetization, specific heat, as well as ESR and μSR techniques. Magnetic susceptibility results suggest that the presence of dominant antiferromagnetic interactions between $S = 3/2$ moments of Cr^{3+} ions along with subdominant ferromagnetic interactions. Specific heat measurements unveil two consecutive phase transitions, one at $T_L = 4.3$ K, corresponding to the canted antiferromagnetic phase, and another at $T_H = 8$ K due to an antiferromagnetic phase. Above T_H, the existence of short-range magnetic correlation is supported by the observation of maximum entropy release and the manifestation of critical-like behavior in the ESR linewidth. Furthermore, μSR provides concrete evidence of the presence of static and dynamic local magnetic fields, particularly below T_L, as well as a critical slowing down of spin dynamics above T_L and persistent spin dynamics to the lowest temperatures. Further investigations on single crystals is essential to gain a detailed understanding of the low-energy excitations associated to the short-range order above the transition temperature and the multistage spin dynamics in this three-dimensional frustrated magnet.

[1] L. Balents, Spin liquids in frustrated magnets, Nature (London) **464**, 199 (2010).

[2] N. D. Mermin and H. Wagner, Absence of ferromagnetism or antiferromagnetism in one- or two-dimensional isotropic Heisenberg models, Phys. Rev. Lett. **17**, 1133 (1966).

[3] P. Khuntia, Novel magnetism and spin dynamics of strongly correlated electron systems: Microscopic insights, J. Magn. Magn. Mater. **489**, 165435 (2019).

[4] J. Khatua, B. Sana, A. Zorko, M. Gomilšek, K. Sethupathi, M. R. Rao, M. Baenitz, B. Schmidt, and P. Khuntia, Experimental signatures of quantum and topological states in frustrated magnetism, Phys. Rep. **1041**, 1 (2023).

[5] Y. Zhou, K. Kanoda, and T.-K. Ng, Quantum spin liquid states, Rev. Mod. Phys. **89**, 025003 (2017).

[6] J. Wen, S.-L. Yu, S. Li, W. Yu, and J.-X. Li, Experimental identification of quantum spin liquids, npj Quantum Mater. **4**, 12 (2019).

[7] L. Savary and L. Balents, Quantum spin liquids: a review, Rep. Prog. Phys. **80**, 016502 (2017).

[8] C. Broholm, R. J. Cava, S. A. Kivelson, D. G. Nocera, M. R. Norman, and T. Senthil, Quantum spin liquids, Science **367**, eaay0668 (2020).

[9] P. W. Anderson, Resonating valence bonds: A new kind of insulator? Mater. Res. Bull. **8**, 153 (1973).

[10] X. G. Wen, Mean-field theory of spin-liquid states with finite energy gap and topological orders, Phys. Rev. B **44**, 2664 (1991).

[11] G. Baskaran, Z. Zou, and P. Anderson, The resonating valence bond state and high-T_c superconductivity—A mean field theory, Solid State Commun. **63**, 973 (1987).

[12] P. W. Anderson, The resonating valence bond state in La_2CuO_4 and superconductivity, Science **235**, 1196 (1987).

[13] H.-C. Jiang and S. A. Kivelson, High temperature superconductivity in a lightly doped quantum spin liquid, Phys. Rev. Lett. **127**, 097002 (2021).

[14] E. Fradkin, S. A. Kivelson, and J. M. Tranquada, *Colloquium:* Theory of intertwined orders in high temperature superconductors, Rev. Mod. Phys. **87**, 457 (2015).

[15] C. Castelnovo, R. Moessner, and S. Sondhi, Spin ice, fractionalization, and topological order, Annu. Rev. Condens. Matter Phys. **3**, 35 (2012).

[16] C. Nayak, S. H. Simon, A. Stern, M. Freedman, and S. Das Sarma, Non-Abelian anyons and topological quantum computation, Rev. Mod. Phys. **80**, 1083 (2008).

[17] P. W. Phillips, L. Yeo, and E. W. Huang, Exact theory for superconductivity in a doped Mott insulator, Nat. Phys. **16**, 1175 (2020).

[18] B. Göbel, I. Mertig, and O. A. Tretiakov, Beyond skyrmions: Review and perspectives of alternative magnetic quasiparticles, Phys. Rep. **895**, 1 (2021).

[19] S. Jeon, D. Wulferding, Y. Choi, S. Lee, K. Nam, K. H. Kim, M. Lee, T.-H. Jang, J.-H. Park, S. Lee *et al.*, One-ninth magnetization plateau stabilized by spin entanglement in a kagome antiferromagnet, Nat. Phys. **20**, 435 (2024).

[20] T. Arh, B. Sana, M. Pregelj, P. Khuntia, Z. Jagličić, M. D. Le, P. K. Biswas, P. Manuel, L. Mangin-Thro, A. Ozarowski, and A. Zorko, The Ising triangular-lattice antiferromagnet neodymium heptatantalate as a quantum spin liquid candidate, Nat. Mater. **21**, 416 (2022).

[21] P. Khuntia, F. Bert, P. Mendels, B. Koteswararao, A. V. Mahajan, M. Baenitz, F. C. Chou, C. Baines, A. Amato, and Y. Furukawa, Spin liquid state in the 3D frustrated antiferromagnet $PbCuTe_2O_6$: NMR and Muon spin relaxation studies, Phys. Rev. Lett. **116**, 107203 (2016).

[22] S. Chillal, Y. Iqbal, H. O. Jeschke, J. A. Rodriguez-Rivera, R. Bewley, P. Manuel, D. Khalyavin, P. Steffens, R. Thomale, A. T. M. N. Islam, J. Reuther, and B. Lake, Evidence for a three-dimensional quantum spin liquid in $PbCuTe_2O_6$, Nat. Commun. **11**, 2348 (2020).

[23] A. C. Shockley, F. Bert, J.-C. Orain, Y. Okamoto, and P. Mendels, Frozen state and spin liquid physics in

Na$_4$Ir$_3$O$_8$: An NMR study, Phys. Rev. Lett. **115**, 047201 (2015).

[24] R. Dally, T. Hogan, A. Amato, H. Luetkens, C. Baines, J. Rodriguez-Rivera, M. J. Graf, and S. D. Wilson, Short-range correlations in the magnetic ground state of Na$_4$Ir$_3$O$_8$, Phys. Rev. Lett. **113**, 247601 (2014).

[25] K. W. Plumb, H. J. Changlani, A. Scheie, S. Zhang, J. W. Krizan, J. A. Rodriguez-Rivera, Y. Qiu, B. Winn, R. J. Cava, and C. L. Broholm, Continuum of quantum fluctuations in a three-dimensional $S = 1$ Heisenberg magnet, Nat. Phys. **15**, 54 (2019).

[26] J. W. Krizan and R. J. Cava, NaCaNi$_2$F$_7$: A frustrated high-temperature pyrochlore antiferromagnet with $S = 1$Ni^{2+}, Phys. Rev. B **92**, 014406 (2015).

[27] Y. Cai, M. N. Wilson, A. M. Hallas, L. Liu, B. A. Frandsen, S. R. Dunsiger, J. W. Krizan, R. J. Cava, O. Rubel, Y. J. Uemura, and G. M. Luke, μSR study of spin freezing and persistent spin dynamics in NaCaNi$_2$F$_7$, J. Condens. Matter Phys. **30**, 385802 (2018).

[28] B. Gao, T. Chen, D. W. Tam, C.-L. Huang, K. Sasmal, D. T. Adroja, F. Ye, H. Cao, G. Sala, M. B. Stone *et al.*, Experimental signatures of a three-dimensional quantum spin liquid in effective spin-1/2 Ce$_2$Zr$_2$O$_7$ pyrochlore, Nat. Phys. **15**, 1052 (2019).

[29] J. Khatua, S. Bhattacharya, Q. P. Ding, S. Vrtnik, A. M. Strydom, N. P. Butch, H. Luetkens, E. Kermarrec, M. S. R. Rao, A. Zorko, Y. Furukawa, and P. Khuntia, Spin liquid state in a rare-earth hyperkagome lattice, Phys. Rev. B **106**, 104404 (2022).

[30] S. Kivelson and S. Sondhi, 50 years of quantum spin liquids, Nat. Rev. Phys. **5**, 368 (2023).

[31] T. Lancaster, Quantum spin liquids, Contemp. Phys. **64**, 127 (2023).

[32] J. Khatua, M. Gomilŝek, J. C. Orain, A. M. Strydom, Z. Jagliĉiĉ, C. V. Colin, S. Petit, A. Ozarowski, L. Mangin-Thro, K. Sethupathi, M. S. R. Rao, A. Zorko, and P. Khuntia, Signature of a randomness-driven spin-liquid state in a frustrated magnet, Commun. Phys. **5**, 99 (2022).

[33] L. T. Nguyen and R. J. Cava, Hexagonal perovskites as quantum materials, Chem. Rev. **121**, 2935 (2021).

[34] C. Bradley and A. Cracknell, *The Mathematical Theory of Symmetry in Solids: Representation Theory for Point Groups and Space Groups* (Oxford University Press, Oxford, 2010).

[35] M. Kakihana, K. Nishimura, Y. Ashitomi, T. Yara, D. Aoki, A. Nakamura, F. Honda, M. Nakashima, Y. Amako, Y. Uwatoko *et al.*, Unique electronic states in non-centrosymmetric cubic compounds, J. Electron. Mater. **46**, 3572 (2017).

[36] T. E. Redpath and J. M. Hopkinson, Spin ice on the trillium lattice studied by Monte Carlo calculations, Phys. Rev. B **82**, 014410 (2010).

[37] V. A. Chizhikov and V. E. Dmitrienko, Multishell contribution to the Dzyaloshinskii-Moriya spiraling in MnSI-type crystals, Phys. Rev. B **88**, 214402 (2013).

[38] I. E. Dzyaloshinskii, Theory of helicoidal structures in antiferromagnets. I. Nonmetals, J. Exptl. Theoret. Phys. (U.S.S.R.) **47**, 336 (1964) [Sov. Phys. JETP **19**, 960 (1964)].

[39] L. Ding, X. Xu, H. O. Jeschke, X. Bai, E. Feng, A. S. Alemayehu, J. Kim, F.-T. Huang, Q. Zhang, X. Ding *et al.*, Field-tunable toroidal moment in a chiral-lattice magnet, Nat. Commun. **12**, 5339 (2021).

[40] M. Ramakrishnan, E. Constable, A. Cano, M. Mostovoy, J. S. White, N. Gurung, E. Schierle, S. d. Brion, C. V. Colin, F. Gay *et al.*, Field-induced double spin spiral in a frustrated chiral magnet, npj Quantum Mater. **4**, 60 (2019).

[41] Y. A. Izyumov, Modulated, or long-periodic, magnetic structures of crystals, Sov. Phys. Uspekhi **27**, 845 (1984).

[42] F. Qian, L. J. Bannenberg, H. Wilhelm, G. Chaboussant, L. M. Debeer-Schmitt, M. P. Schmidt, A. Aqeel, T. T. M. Palstra, E. Brück, A. J. E. Lefering *et al.*, New magnetic phase of the chiral skyrmion material Cu$_2$OSeO$_3$, Sci. Adv. **4**, eaat7323 (2018).

[43] S. Mühlbauer, B. Binz, F. Jonietz, C. Pfleiderer, A. Rosch, A. Neubauer, R. Georgii, and P. Böni, Skyrmion lattice in a chiral magnet, Science **323**, 915 (2009).

[44] X. Z. Yu, N. Kanazawa, Y. Onose, K. Kimoto, W. Z. Zhang, S. Ishiwata, Y. Matsui, and Y. Tokura, Near room-temperature formation of a skyrmion crystal in thin-films of the helimagnet FeGe, Nat. Mater. **10**, 106 (2011).

[45] N. Kanazawa, Y. Onose, T. Arima, D. Okuyama, K. Ohoyama, S. Wakimoto, K. Kakurai, S. Ishiwata, and Y. Tokura, Large topological Hall effect in a short-period helimagnet MnGe, Phys. Rev. Lett. **106**, 156603 (2011).

[46] N. Higa, T. U. Ito, M. Yogi, T. Hattori, H. Sakai, S. Kambe, Z. Guguchia, W. Higemoto, M. Nakashima, Y. Homma, A. Nakamura, F. Honda, Y. Shimizu, D. Aoki, M. Kakihana, M. Hedo, T. Nakama, Y. Ōnuki, and Y. Tokunaga, Critical slowing-down and field-dependent paramagnetic fluctuations in the skyrmion host EuPtSi: μSR and NMR studies, Phys. Rev. B **104**, 045145 (2021).

[47] F. Kneidinger, I. Zeiringer, A. Siderenko, E. Bauer, H. Michor, P. Rogl, and J. G. Sereni, Physical properties of CeIrSi with trillium-lattice frustrated magnetism, Phys. Rev. B **100**, 134442 (2019).

[48] C. Pfleiderer, G. J. McMullan, S. R. Julian, and G. G. Lonzarich, Magnetic quantum phase transition in MnSi under hydrostatic pressure, Phys. Rev. B **55**, 8330 (1997).

[49] J. M. Hopkinson and H.-Y. Kee, Geometric frustration inherent to the trillium lattice, a sublattice of the B20 structure, Phys. Rev. B **74**, 224441 (2006).

[50] I. Živković, V. Favre, C. Salazar Mejia, H. O. Jeschke, A. Magrez, B. Dabholkar, V. Noculak, R. S. Freitas, M. Jeong, N. G. Hegde, L. Testa, P. Babkevich, Y. Su, P. Manuel, H. Luetkens, C. Baines, P. J. Baker, J. Wosnitza, O. Zaharko, Y. Iqbal *et al.*, Magnetic field induced quantum spin liquid in the two coupled trillium lattices of K$_2$Ni$_2$(SO$_4$)$_3$, Phys. Rev. Lett. **127**, 157204 (2021).

[51] W. Yao, Q. Huang, T. Xie, A. Podlesnyak, A. Brassington, C. Xing, R. S. D. Mudiyanselage, H. Wang, W. Xie, S. Zhang, M. Lee, V. S. Zapf, X. Bai, D. A. Tennant, J. Liu, and H. Zhou, Continuous spin excitations in the three-dimensional frustrated magnet K$_2$Ni$_2$(SO$_4$)$_3$, Phys. Rev. Lett. **131**, 146701 (2023).

[52] K. Boya, K. Nam, K. Kargeti, A. Jain, R. Kumar, S. K. Panda, S. M. Yusuf, P. L. Paulose, U. K. Voma, E. Kermarrec *et al.*, Signatures of spin-liquid state in a 3D frustrated lattice compound KSrFe$_2$(PO$_4$)$_3$ with S = 5/2, APL Mater. **10**, 101103 (2022).

[53] J. M. Bulled, J. A. M. Paddison, A. Wildes, E. Lhotel, S. J. Cassidy, B. Pato-Doldán, L. C. Gómez-Aguirre, P. J. Saines,

and A. L. Goodwin, Geometric frustration on the trillium lattice in a magnetic metal-organic framework, Phys. Rev. Lett. **128**, 177201 (2022).

[54] X. Huai and T. T. Tran, Design principles for noncentrosymmetric materials, Annu. Rev. Mater. Res. **53**, 253 (2023).

[55] A. E. Hall, P. Manuel, D. D. Khalyavin, F. Orlandi, D. A. Mayoh, L.-J. Chang, Y.-S. Chen, D. G. C. Jonas, M. R. Lees, and G. Balakrishnan, Comparative study of the magnetism in Mn_3RhGe and related compound Mn_3IrSi, Phys. Rev. Mater. **7**, 114402 (2023).

[56] A. Suter and B. M. Wojek, Musrfit: A free platform-independent framework for μSR data analysis, Phys. Procedia **30**, 69 (2012).

[57] B. H. Toby, *EXPGUI*, a graphical user interface for *GSAS*, J. Appl. Crystallogr. **34**, 210 (2001).

[58] J. Isasi and A. Daidouh, Synthesis, structure and conductivity study of new monovalent phosphates with the langbeinite structure, Solid State Ion. **133**, 303 (2000).

[59] A. Boudjada and R. Perret, Crystal data for the two triple monophosphates $K_2CrTi(PO_4)_3$ and $Ba_2MgCr(PO_4)_3$, J. Appl. Crystallogr. **10**, 129 (1977).

[60] S. T. Norberg, New phosphate langbeinites, $K_2MTi(PO_4)_3$ ($M = $ Er, Yb or Y), and an alternative description of the langbeinite framework, Acta Crystallogr. Sec. B **58**, 743 (2002).

[61] S. V. Isakov, J. M. Hopkinson, and H.-Y. Kee, Fate of partial order on trillium and distorted windmill lattices, Phys. Rev. B **78**, 014404 (2008).

[62] K. Tustain, B. Ward-O'Brien, F. Bert, T. Han, H. Luetkens, T. Lancaster, B. M. Huddart, P. J. Baker, and L. Clark, From magnetic order to quantum disorder in the Zn-barlowite series of S = 1/2 kagomé antiferromagnets, npj Quantum Mater. **5**, 74 (2020).

[63] M. S. Khan, A. Bandyopadhyay, A. Nag, V. Kumar, A. V. Mahajan, and S. Ray, Magnetic ground state of the distorted 6H perovskite $Ba_3CdIr_2O_9$, Phys. Rev. B **100**, 064423 (2019).

[64] T. Zhu, S. Lee, X. Zhang, H. Yang, Y. Jin, Y. Jin, K.-Y. Choi, and M. Lü, Variable structures and one-dimensional-canting antiferromagetism found in fluoride selenates, $A_2Mn(SeO_4)F_3$ (A = K, Rb, Cs), Inorg. Chem. **60**, 13707 (2021).

[65] Z. Bukowski, D. Rybicki, M. Babij, J. Przewoźnik, Ł. Gondek, J. Żukrowski, and C. Kapusta, Canted antiferromagnetic order in $EuZn_2As_2$ single crystals, Sci. Rep. **12**, 14718 (2022).

[66] Y. Lai, L. Ke, J. Yan, R. D. McDonald, and R. J. McQueeney, Defect-driven ferrimagnetism and hidden magnetization in $MnBi_2Te_4$, Phys. Rev. B **103**, 184429 (2021).

[67] J. A. Sannes and M. Valldor, $Sr_2Te_4V_2O_{13}Cl_2$, a layered structure forming a canted antiferromagnetic ground state, Chem. Mater. **36**, 2355 (2024).

[68] X. Liu, K. M. Taddei, S. Li, W. Liu, N. Dhale, R. Kadado, D. Berman, C. D. Cruz, and B. Lv, Canted antiferromagnetism in the quasi-one-dimensional iron chalcogenide $BaFe_2Se_4$, Phys. Rev. B **102**, 180403(R) (2020).

[69] S. Boseggia, R. Springell, H. C. Walker, A. T. Boothroyd, D. Prabhakaran, D. Wermeille, L. Bouchenoire, S. P. Collins, and D. F. McMorrow, Antiferromagnetic order and domains in $Sr_3Ir_2O_7$ probed by x-ray resonant scattering, Phys. Rev. B **85**, 184432 (2012).

[70] G. Cao, A. Subedi, S. Calder, J.-Q. Yan, J. Yi, Z. Gai, L. Poudel, D. J. Singh, M. D. Lumsden, A. D. Christianson, B. C. Sales, and D. Mandrus, Magnetism and electronic structure of

La_2ZnIrO_6 and La_2MgIrO_6: Candidate $J_{eff} = \frac{1}{2}$ Mott insulators, Phys. Rev. B **87**, 155136 (2013).

[71] A. Verrier, F. Bert, J. M. Parent, M. El-Amine, J. C. Orain, D. Boldrin, A. S. Wills, P. Mendels, and J. A. Quilliam, Canted antiferromagnetic order in the kagome material Sr-vesignieite, Phys. Rev. B **101**, 054425 (2020).

[72] B. Schmidt and P. Thalmeier, Frustrated two dimensional quantum magnets, Phys. Rep. **703**, 1 (2017), Frustrated two dimensional quantum magnets.

[73] S. Kimura, S. Imajo, M. Gen, T. Momoi, M. Hagiwara, H. Ueda, and Y. Kohama, Quantum phase of the chromium spinel oxide $HgCr_2O_4$ in high magnetic fields, Phys. Rev. B **105**, L180405 (2022).

[74] I. L. Danilovich, A. V. Merkulova, I. V. Morozov, E. A. Ovchenkov, F. M. Spiridonov, E. A. Zvereva, O. S. Volkova, V. V. Mazurenko, Z. V. Pchelkina, A. A. Tsirlin *et al.*, Strongly canted antiferromagnetic ground state in $Cu_3(OH)_2F_4$, J. Alloys Compd. **776**, 16 (2019).

[75] M. Bałanda, AC susceptibility studies of phase transitions and magnetic relaxation: Conventional, molecular and low-dimensional magnets, Acta Phys. Pol. A **124**, 964 (2013).

[76] M. A. Gîrţu, C. M. Wynn, W. Fujita, K. Awaga, and A. J. Epstein, Glassiness and canted antiferromagnetism in three geometrically frustrated triangular quantum Heisenberg antiferromagnets with additional Dzyaloshinskii-Moriya interaction, Phys. Rev. B **61**, 4117 (2000).

[77] J. Khatua, T. Arh, S. B. Mishra, H. Luetkens, A. Zorko, B. Sana, M. S. R. Rao, B. R. K. Nanda, and P. Khuntia, Development of short and long-range magnetic order in the double perovskite based frustrated triangular lattice antiferromagnet Ba_2MnTeO_6, Sci. Rep. **11**, 6959 (2021).

[78] G. S. Murugan, C. Lee, R. Kalaivanan, I. P. Muthuselvam, Y. Oshima, K.-Y. Choi, and R. Sankar, Anomalous spin dynamics of the $S = \frac{3}{2}$ kagome ferromagnet $Li_9Cr_3(P_2O_7)_3(PO_4)_2$, Phys. Rev. B **107**, 214411 (2023).

[79] S. Lee, T. Zhu, Y. Oshima, T. Shiroka, C. Wang, H. Luetkens, H. Yang, M. Lü, and K.-Y. Choi, Timescale distributions of spin fluctuations in the $S = 2$ kagome antiferromagnet $CsMn_3F_6(SeO_3)_2$, Phys. Rev. B **105**, 094439 (2022).

[80] A. Abragam and B. Bleaney, *Electron Paramagnetic Resonance of Transition Ions* (Clarendon Press, Oxford, 1970).

[81] A. Glamazda, Y. S. Choi, S.-H. Do, S. Lee, P. Lemmens, A. N. Ponomaryov, S. A. Zvyagin, J. Wosnitza, D. P. Sari, I. Watanabe, and K.-Y. Choi, Quantum criticality in the coupled two-leg spin ladder Ba_2CuTeO_6, Phys. Rev. B **95**, 184430 (2017).

[82] S. Lee, S.-H. Do, W.-J. Lee, Y. S. Choi, M. Lee, E. S. Choi, A. P. Reyes, P. L. Kuhns, A. Ozarowski, and K.-Y. Choi, Multistage symmetry breaking in the breathing pyrochlore lattice $Li(Ga, In)Cr_4O_8$, Phys. Rev. B **93**, 174402 (2016).

[83] A. Yaouanc and P. D. De Reotier, *Muon Spin Rotation, Relaxation, and Resonance: Applications to Condensed Matter*, (Oxford University Press, Oxford, 2011).

[84] E. Nocerino, S. Kobayashi, C. Witteveen, O. K. Forslund, N. Matsubara, C. Tang, T. Matsukawa, A. Hoshikawa, A. Koda, K. Yoshimura *et al.*, Competition between magnetic interactions and structural instabilities leading to itinerant frustration in the triangular lattice antiferromagnet $LiCrSe_2$, Commun. Mater. **4**, 81 (2023).

[85] K. Papadopoulos, O. K. Forslund, E. Nocerino, F. O. L. Johansson, G. Simutis, N. Matsubara, G. Morris, B. Hitti, D. Arseneau, P. Svedlindh, M. Medarde, D. Andreica, J.-C. Orain, V. Pomjakushin, L. Börjesson, J. Sugiyama, M. Månsson, and Y. Sassa, Influence of the magnetic sublattices in the double perovskite LaCaNiReO$_6$, Phys. Rev. B **106**, 214410 (2022).

[86] I. A. Campbell, A. Amato, F. N. Gygax, D. Herlach, A. Schenck, R. Cywinski, and S. H. Kilcoyne, Dynamics in canonical spin glasses observed by muon spin depolarization, Phys. Rev. Lett. **72**, 1291 (1994).

[87] A. Yaouanc, P. Dalmas de Réotier, Y. Chapuis, C. Marin, G. Lapertot, A. Cervellino, and A. Amato, Short-range magnetic ordering process for the triangular-lattice compound NiGa$_2$S$_4$: A positive muon spin rotation and relaxation study, Phys. Rev. B **77**, 092403 (2008).

[88] C. Koo, J. Werner, M. Tzschoppe, M. Abdel-Hafiez, P. K. Biswas, R. Sarkar, H.-H. Klauss, G. V. Raganyan, E. A. Ovchenkov, A. Y. Nikulin, A. N. Vasiliev, E. A. Zvereva, and R. Klingeler, Magnetism and the phase diagram of MnSb$_2$O$_4$, Phys. Rev. B **97**, 224416 (2018).

[89] T. Weinhold, C. Wang, F. Seewald, V. Grinenko, Y. Imai, F. Sato, K. Ohgushi, H.-H. Klauss, and R. Sarkar, Magnetism in the Kitaev quantum spin liquid candidate RuBr$_3$, Phys. Rev. B **109**, 014440 (2024).

[90] Y. Li, Q.-Y. Li, W. Li, T. Liu, D. J. Voneshen, P. K. Biswas, and D. Adroja, Spin dynamics and Griffiths singularity in the random quantum Ising magnet PrTiNbO$_6$, npj Quantum Mater. **6**, 34 (2021).

[91] P. Khuntia, S. Manni, F. R. Foronda, T. Lancaster, S. J. Blundell, P. Gegenwart, and M. Baenitz, Local magnetism and spin dynamics of the frustrated honeycomb rhodate Li$_2$RhO$_3$, Phys. Rev. B **96**, 094432 (2017).

[92] A. Zorko, F. Bert, P. Mendels, K. Marty, and P. Bordet, Ground state of the easy-axis rare-earth kagome langasite Pr$_3$Ga$_5$SiO$_{14}$, Phys. Rev. Lett. **104**, 057202 (2010).

[93] D. R. Noakes and G. M. Kalvius, Anomalous zero-field muon spin relaxation in highly disordered magnets, Phys. Rev. B **56**, 2352 (1997).

[94] S.-H. Do, W.-J. Lee, S. Lee, Y. S. Choi, K.-J. Lee, D. I. Gorbunov, J. Wosnitza, B. J. Suh, and K.-Y. Choi, Short-range quasistatic order and critical spin correlations in α-Ru$_{1-x}$Ir$_x$Cl$_3$, Phys. Rev. B **98**, 014407 (2018).

[95] S. Lee, Y. S. Choi, S.-H. Do, W. Lee, C. H. Lee, M. Lee, M. Vojta, C. N. Wang, H. Luetkens, Z. Guguchia, and K.-Y. Choi, Kondo screening in a Majorana metal, Nat. Commun. **14**, 7405 (2023).

[96] P. J. Baker, I. Franke, F. L. Pratt, T. Lancaster, D. Prabhakaran, W. Hayes, and S. J. Blundell, Probing magnetic order in LiMPO$_4$ (M = Ni, Co, Fe) and lithium diffusion in Li$_x$FePO$_4$, Phys. Rev. B **84**, 174403 (2011).

[97] O. K. Forslund, K. Papadopoulos, E. Nocerino, G. Morris, B. Hitti, D. Arseneau, V. Pomjakushin, N. Matsubara, J.-C. Orain, P. Svedlindh, D. Andreica, S. Jana, J. Sugiyama, M. Månsson, and Y. Sassa, Intertwined magnetic sublattices in the double perovskite compound LaSrNiReO$_6$, Phys. Rev. B **102**, 144409 (2020).

[98] J. A. Hodges, P. Bonville, A. Forget, A. Yaouanc, P. Dalmas de Réotier, G. André, M. Rams, K. Królas, C. Ritter, P. C. M. Gubbens, C. T. Kaiser, P. J. C. King, and C. Baines, First-order transition in the spin dynamics of geometrically frustrated Yb$_2$Ti$_2$O$_7$, Phys. Rev. Lett. **88**, 077204 (2002).

[99] S. Lee, S.-H. Do, W. Lee, Y. S. Choi, J. van Tol, A. P. Reyes, D. Gorbunov, W.-T. Chen, and K.-Y. Choi, Dichotomy in temporal and thermal spin correlations observed in the breathing pyrochlore LiGa$_{1-x}$In$_x$Cr$_4$O$_8$, npj Quantum Mater. **6**, 47 (2021).

[100] B. A. Frandsen, K. A. Petersen, N. A. Ducharme, A. G. Shaw, E. J. Gibson, B. Winn, J. Yan, J. Zhang, M. E. Manley, and R. P. Hermann, Spin dynamics and a nearly continuous magnetic phase transition in an entropy-stabilized oxide antiferromagnet, Phys. Rev. Mater. **4**, 074405 (2020).

Correction: Two author names were missing in the original publication and have been inserted as the seventh and eighth authors. The associated institution has been inserted as the sixth affiliation.